Journal of Applied Phycology
https://doi.org/10.1007/s10811-021-02591-0

Temperature-induced response in algal cell surface properties and behaviour: an experimental approach

N. Novosel[1] · T. Mišić Radić[1] · J. Zemla[2] · M. Lekka[2] · A. Čačković[1] · D. Kasum[1] · T. Legović[1,3,4] · P. Žutinić[5] · M. Gligora Udovič[5] · N. Ivošević DeNardis[1]

Received: 18 February 2021 / Revised and accepted: 12 August 2021

Abstract
Microalgae are considered an accurate indicator of ecosystem perturbations induced by global climate change. The present work aims to investigate the alteration of temperature on surface properties and behaviour of three algal species using the complementary surface methods (electrochemical and atomic force microscopy). The results showed that the temperature-induced response of algae is species-specific due to the structural features of the cell envelope. Wall-less algae experience the largest nanomechanical and chemical change, while algae with silicified walls show the pronounced chemical change in the degree of hydrophobicity. Alterations of surface properties suggest a molecular modification of the algal barrier and cytoskeletal rearrangements due to a change in cell size, while algal morphology reveals no change. The physiological activity of cells showed a different organisation of released extracellular substances in the form of fine fibrillar structures, aggregated particles, and dense networks. Both types of algal responses, physiological activity, and molecular modification of the cell barrier determine the cell adhesion and motility. This study highlights the role of surface properties in cell-substrate and cell–cell interactions, which is important for the understanding of algal behaviour at natural interfaces and the mechanism of algal biofilm and aggregate formation in aquatic systems under the stress.

Keywords Algae · Adhesion · Hydrophobicity · Morphology · Motility · Stiffness

Introduction

Marine microalgae support about half of the global primary production, drive essential biogeochemical cycles, and form the basis of the aquatic food web. Their short life cycle enables them to respond rapidly to climate change or the presence of pollutants (Beaugrand 2005; Hays et al. 2005). The slight change in environmental factors such as light, nutrients, pH, and temperature influences the growth rate and productivity of microalgae (Falkowski and Raven 2007).

✉ N. Ivošević DeNardis
ivosevic@irb.hr

1 Ruđer Bošković Institute, Zagreb, Croatia

2 Institute of Nuclear Physics Polish Academy of Sciences, Kraków, Poland

3 Libertas International University, Zagreb, Croatia

4 OIKON-Institute for Applied Ecology, Zagreb, Croatia

5 Department of Biology, Faculty of Science, University of Zagreb, Zagreb, Croatia

Temperature is one of the key factors that directly affects various cell physiological processes, e.g. biomass production, metabolic reactions, respiration, photosynthesis, and ecological interactions (Lewandowska and Sommer 2010; Guinder and Molinero 2013). An increase in temperature in the water column caused by higher solar radiation leads to oxidative stress of algal cells (Roncarati et al. 2008; Huertas et al. 2011; Häder and Gao 2015). As an adaptive response to environmental conditions, algae can adjust membrane fluidity by altering fatty acid saturation levels, reduce protein synthesis to avoid an increase in misfolded proteins, accumulate compatible solutes to maintain cell osmolarity, regulate photosynthesis to balance energy production and consumption (Barati et al. 2019, Pavlinska et al. 2020), and release extracellular polymeric substances (EPS; Decho and Gutierrez 2017; Kumar et al. 2017).

We focused on the biointerface (i.e. algal cell envelope) that separates cells from the external medium and where complex processes occur simultaneously. The surface properties of the biointerface are responsible for the behaviour, fate, and role of cells in aquatic systems (Klenerman

Published online: 22 October 2021

et al. 2011). Our previous studies showed that the surface properties of algal cells are subject to change during the growth phase (Pillet et al. 2019). In the exponential phase, *Dunaliella tertiolecta* cells were stiffer and hydrophobic, while algae became softer and hydrophilic in the stationary phase. Such alterations of algal surface properties were considered to reflect molecular modification of the cell envelope. Changes in the surface properties of algae consequently reflect on the adhesion kinetics of algae at the model charged interface. The alteration of surface properties, morphology, and physiological activity were determined when algae were exposed to heavy metal cadmium (Ivošević DeNardis et al. 2019). *Dunaliella tertiolecta* cells became stiffer due to the expression of surface proteins, such as chlorophyll *a-b* binding protein and carbonic anhydrase, which are responsible for maintaining the photosystem (Lane et al. 2005). The frustule of *Cylindrotheca closterium* showed nanomorphological changes accompanied by enhancing organic matter production as a feedback response to the heavy metal of cadmium (Mišić Radić et al. 2020).

Microalgal responses to temperature variations have been examined at different spatiotemporal scales, both in empirical and field investigations, as well as using modelling approaches (Sarmiento et al. 2004; Boyce et al. 2010; Huertas et al. 2011). A number of recent studies have investigated the effect of temperature on algal growth and surface properties for applicative usage (Ozkan and Berberoglu 2013; Ras et al. 2013; Gross et al. 2016; Xia et al. 2017; Ahmad et al. 2020). However, the comprehensive biophysical examination of algae on the single-cell level focusing on biointerface and the ecological implications of the aforementioned interaction have been poorly explored.

This study aims to investigate the temperature-induced response in the surface properties and behaviour of three widely distributed marine algal species, taking into account their structural features that can contribute to temperature tolerance. We selected the biflagellate green alga *D. tertiolecta* with a mucous plasma membrane called a glycocalyx, the tetraflagellate green alga *Tetraselmis suecica* enveloped within a calcite-encrusted theca, and the gliding diatom *C. closterium* with a rigid organosilicate cell wall to be examined at selected temperatures simulating the annual variations in aquatic systems. We will combine complementary surface method approach such as electrochemical methods and atomic force microscopy. High-resolution imaging will enable the visualisation of structural details of the cell surface and the organisation of the released biopolymers at the molecular level. Nanomechanical measurements will determine the physicochemical properties of the cells (e.g. elasticity and adhesion). The electrochemical measurements will determine the adhesion behaviour of the cell at the interface as a consequence of material fluidity and hydrophobicity and the content of released surface-active matter. Cell motility will be analysed in terms of cell speed and search radius, both of which reflect the physiological state of the cell. This study, conducted in batch cultures under controlled laboratory conditions, will enable a better understanding of algal responses to the temperature shifts induced by climate change.

Materials and methods

Cell suspensions

Three marine algal species used were *Dunaliella tertiolecta* (DT, Chlorophyceae, CCMP 1320, Culture Collection Bigelow Laboratory for Ocean Sciences, Bigelow, MN, USA), *Tetraselmis suecica* (TS, Chlorophyceae, CCAP 66/22A, Collection of Algae and Protozoa, Scottish Marine Institute, Oban UK), and *Cylindrotheca closterium* (CC, Bacillariophyceae, CCMP 1554, Culture Collection Bigelow Laboratory for Ocean Sciences, Bigelow, MN, USA). Cells were cultured in natural seawater (salinity of 38 ‰) filtered through a pore size of 0.22 µm and enriched with F/2 growth medium (Guillard 1975). Cultures were maintained in a water bath with constant shaking (20 rpm) under a 12:12 light:dark cycle with an irradiance of 31 µmol photons m^{-2} s^{-1}. Algal species were cultured at three selected temperatures of 12 °C, 18 °C, and 30 °C. Between each temperature change, cells were acclimated at 18 °C for 14 days before exposure at 12 °C and 30 °C. The average cell abundance was determined in three sample replicates using Fuchs-Rosenthal haemocytometer (Fein-Optik Jena, Germany, depth 0.2 mm) and light microscope (Olympus BX51, Olympus Corporation, Japan). The determination of growth rate and duplication time in the exponential growth phase of algal cells were provided by Kim (2015). Cells were harvested at the stationary phase (19 days) by centrifugation (1,500 x*g*, 3 min) followed by rinsing and resuspending pellet twice with filtered seawater. The final pellet was resuspended in 2 mL of filtered seawater and served as the stock suspension.

Motility analysis

Aliquots of cell culture were observed under an Olympus BX51 microscope (10x). Video files of 5 s were recorded 10 times consecutively in the sample (50–60 frames per second, image size: 340 × 250, 4 × 4 binning). The video files saved in.avi format were used as input to the open-source image processing software ICY (http:icy.bioimageanalysis.org) to analyse cell motility and trajectories (Novosel et al. 2020). Three plugins were used: Spot Tracking, Track Manager, and Motion Profiler. Data from the analyses of 1000 cells were imported into Microsoft Excel (Microsoft Corporation, Redmond, WA, USA). The output of ICY is an ASCII

file with row data (sample size, the spatiotemporal position of cells, the number of motile and non-motile cells with the corresponding minimum, median, arithmetic mean, and maximum speeds and search radius). The search radius is the maximum distance from the initial point. Linearity is the ratio between the search distance and total path length. The R software package (R Development Core Team 2020) was used to perform additional statistical analyses that included box plots, plots of probability density distributions of speed and search radius, and the Shapiro and Wilcoxon-Mann–Whitney tests.

Electrochemical method

We used the electrochemical method of polarography and chronoamperometry of oxygen reduction at the dropping mercury electrode (DME). The organic constituents such as biopolymers and fluid microparticles in aqueous electrolyte solution can be classified by their electrochemical responses (Figure S1) based on the phenomena of molecular adsorption or particle adhesion at the DME (Žutić et al. 2004; Svetličić et al. 2006; Pletikapić and Ivošević DeNardis 2017). The adsorption of organic molecules at the DME results in a decrease of the surface tension gradient at the mercury electrode/solution interface, which causes the suppression of convective streaming. A gradual decrease in the oxygen reduction current on the chronoamperometric curve corresponds to biopolymer adsorption, which is proportional to the surfactant concentration in the sample and is called surfactant activity. Surfactant activity can be measured by recording the polarographic maximum of Hg(II) ions and offers an alternative approach to measuring dissolved organic carbon in seawater (Hunter and Liss 1981). The surfactant activity is expressed as the equivalent amount of the nonionic synthetic surfactant Triton-X-100 (polyethylene glycol tert-octylphenyl ether, $MW = 600$) in milligram per litre. In contrast, the adhesion of fluid organic particles causes a transient increase in interfacial turbulence, resulting in the spike-shaped amperometric signals (Kovač et al. 2000; Svetličić et al. 2000, 2001; Ivošević DeNardis et al. 2007). The adhesion of a single organic particle from the suspension to the charged interface is recorded as an amperometric signal. The occurrence of amperometric signals of particles is random due to the spatial heterogeneity inherent to a dispersed system and the stochastic nature of the particles' encounter with the electrode. At constant electrode potential, the current amplitude reflects the size of the adhered particle, while the signal frequency reflects the particle concentration in the suspension (Kovač et al. 2000). Whether the adhesion is spontaneous and how fast it progresses depends on the interfacial properties of the three interfaces in contact (particle-medium-electrode). According to the modified Young–Dupré equation (Israelachvili1992), the total Gibbs energy of the interaction between an organic droplet and the aqueous mercury interface is:

$$-\Delta G = A\left(\gamma_{12} - \gamma_{23} - \gamma_{13}\right) \tag{1}$$

$$-\Delta G = A\, S_{132} \tag{2}$$

where γ_{12}, γ_{13}, and γ_{23} are the interfacial energies at the mercury/water, mercury/organic liquid, and water/organic liquid interfaces. The expression in parentheses is equal to the spreading coefficient at the three-phase boundary S_{132}. When $S_{132} > 0$, the attachment and spreading of organic droplets are spontaneous processes, while when $S_{132} < 0$, spreading is not spontaneous. The critical interfacial tension of adhesion $\left(\gamma_{12}\right)_c$ at the $S_{132} = 0$ is equal to $\gamma_{13} + \gamma_{23}$.

Electrochemical measurements of algal cells

Electrochemical measurements were performed in an air-permeable Metrohm vessel with a three-electrode system. The dropping mercury electrode served as the working electrode (dropping time, 2.0 s; flow rate, 6.0 mg s^{-1}; maximum surface area, 4.57 mm^2). All potentials were referenced to a potential measured at an Ag/AgCl (0.1 M NaCl) reference electrode separated from the measured dispersion by a ceramic frit. Platinum served as the counter electrode. An aliquot of the stock cell suspensions was added to 25 mL of filtered seawater (pH 8.0) and then poured into a thermostatted Metrohm vessel at 20 °C. Electrochemical measurements were conducted using a 174A Polarographic Analyser (Princeton Applied Research, Oak Ridge, TN) connected to a computer. Analogue data acquisition was performed using a DAQ card-AI-16-XE-50 (National Instruments, Austin, TX), and data were analysed using the application developed in LabView 6.1 software (National Instruments). The interaction of cells with the electrode is measured by recording polarograms of oxygen reduction (current–potential curve with a scan rate of 10 mV s^{-1}) and current–time curves over 50 mercury drop lives at constant potentials (time resolution: 50 s). Signal frequency is expressed as the number of amperometric signals over 100 s. The surfactant activity is measured by adding 0.5 mL of 0.1 M $HgCl_2$ to the sample before measurement is taken.

Atomic force microscopy imaging

Atomic force microscopy (AFM) measurements were performed using a multimode scanning probe microscope with a Nanoscope IIIa controller (Bruker, Billerica, MA) with a vertical engagement (JV) 125 µm scanner. For imaging in the air, contact mode using silicon nitride contact mode cantilevers (DNP, Bruker, nominal frequency of 18 kHz, nominal spring constant of 0.06 N m^{-1}) were used throughout the

experiments. The linear scan rate was optimised between 1.5 and 2 Hz with a scan resolution of 512 samples per line. The set point was kept at the lowest possible value to minimise the interaction forces between the tip and the surface. Image processing and analysis were performed using the NanoscopeTM software (Bruker, Billerica, MA, USA).

Sample preparation for AFM imaging of cells and released extracellular polymers

The protocol for cell isolation from the growth medium is described in "Cell suspensions" section. The slightly modified protocol for cell isolation was only used for *T. suecica* grown at 12 °C for AFM measurements. The volume of 40 mL *T. suecica* culture was centrifuged at 4,000 ×*g* for 5 min. The loose pellet was washed twice with filtered seawater and diluted with filtered seawater to a final volume of 5 mL, which served for AFM imaging of the cells and released extracellular polymers. The sample preparation protocol for AFM imaging required the fixation of only *D. tertiolecta* stock suspension. *D. tertiolecta* and *C. closterium* were deposited on a bare mica surface, while for *T. suecica*, mica surface was modified with polyethyleneimine (PEI; Sigma-Aldrich Corporation, St. Louis, MS) because of the pronounced cell movement. A 5-µL aliquot of cell suspension was pipetted onto freshly cleaved mica and placed in a closed Petri dish for 1 h to allow the cells to settle and attach to the surface. The mica was then rinsed by immersing three times in a glass with ultrapure water for 30 s and allowed to dry. Afterwards, it was glued to a metal sample pack with double-sided tape and imaged with AFM. In the case of *T. suecica*, the mica was coated with PEI before the immobilisation of the algal cells as follows. A 50 µL aliquot of 0.2% PEI was placed on a freshly cleaved mica surface and incubated for 30 min. The mica was then washed with ultrapure water and dried with nitrogen followed by the cell deposition procedure described above.

Atomic force microscopy working in force spectroscopy mode

AFM measurements of physicochemical properties (i.e. cell elasticity and adhesion) were performed using the Nanowizard IV AFM system (Bruker-JPK, Germany) equipped with a liquid cell setup. Algal cells were indented with MLCT-D silicon nitride cantilevers, characterised by a nominal spring constant of 0.03 N m^{-1} and half open-angle of 21°. Spring constants of the cantilevers were calibrated using the thermal noise method (Sader et al. 1995). Force curves were recorded in the central area of the cell body within a scan area of 3 µm × 3 µm, within which a grid of 6 × 6 points was set. The force curves were recorded at an approach and retract velocity of 8 μms^{-1}, a maximum force of 4 nN, and curve lengths of 4 µm (*C. closterium* and *T. suecica*) and 6 µm (*D. tertiolecta*). The measurements were performed in seawater at room temperature. Recorded data, i.e. force curves, were analysed using JPK Data Processing Software (Bruker-JPK, Germany).

Young's modulus determination

The apparent Young's modulus value was obtained by applying the Hertz-Sneddon contact model (Sneddon 1965). In our study, we used cantilevers with a tip being a four-sided pyramid. Thus, the following equation was applied to describe the relationship between the load force F and the indentation depth δ:

$$F = \frac{E'}{1-\mu^2}\frac{tana}{\sqrt{2}}\delta^2 \tag{3}$$

where μ is the Poisson's ratio, and α is the open-angle of the cantilever's tip. E' is the reduced Young's modulus given by:

$$\frac{1}{E'} = \frac{1-\mu_{tip}^2}{E_{tip}} + \frac{1-\mu_{cell}^2}{E_{cell}}. \tag{4}$$

When $E_{cell} << E_{tip}$, the following relation is obtained:

$$E' = \frac{E_{cell}}{1-\mu_{cell}^2}, \tag{5}$$

where μ_{cell} and μ_{tip} are Poisson's ratios related to the compressibility of the algal cell and indenting cantilever. In our analysis, Poisson's ratio was set to 0.5, assuming that the algal cells are incompressible. AFM data were fitted to the model over a whole indentation range. However, the maximum indentation depth did not exceed 1 µm. The apparent Young's moduli distributions were presented as box plots, where the median and the first (Q_1) and third (Q_3) quartile values are marked.

To quantify the adhesive and hydrophobic properties of algal cells, the retract part of the force curve was analysed. As a result, a maximum work of adhesion (W_{adh}) was determined, which was defined as the area encompassing the negative force values. The value obtained for bare (unmodified) cantilevers quantifies the adhesive surface properties. To obtain the information on the surface hydrophobicity of cells, cantilevers were modified with a hydrophobic trichlorooctadecylsilane (OTS; Sigma-Aldrich) by chemical vapour deposition. Silanisation of the cantilevers was performed in a desiccator for 2 h. Each set of AFM experiments was performed with newly prepared cantilevers that were used immediately after OTS deposition. Thirty-six force curves over 3 µm × 3 µm of the cell body were collected at a

velocity of 8 µm s^{-1} and the maximum load force of 4 nN. The number of cells examined varied from 20 to 30 per case.

The difference between the maximum work of adhesion, extracted from force curves collected with bare and CH_3-functionalised AFM cantilevers, determined the algal cell hydrophobicity level:

$$\Delta W_{adh} = W_{adh(noOTS)} - W_{adh(OTS)} \quad (6)$$

Sample preparation for force spectroscopy measurements

To prepare samples for AFM force spectroscopy measurements, the following protocol was applied. First, 1.5 mL of suspensions of *D. tertiolecta* and *T. suecica* were centrifuged for 3 min at 265 x*g* and for 5 min at 940 x*g*, respectively. Then, 1 mL of the medium was removed, and a pellet of the algal cells was vortexed. After that, 1 mL of filtered seawater was added, and the cells were centrifuged again at the same speed and time. The supernatant was removed, and the cells were suspended in 400 µL of the filtered seawater. A glass coverslip with a PEI coated surface was used as a substrate. PEI was deposited on a glass slide using the drop-casting technique for 1 h and then subsequently dried with a stream of nitrogen. Afterwards, 100 µL of cell suspension was placed for 30 min. Later, the samples were rinsed 3 times, with 100 µL of the filtered seawater. Finally, the samples were covered with seawater, and AFM experiments were performed. *C. closterium* cells (100 µL) were immobilised on a microscopic glass slide cleaned with an oxygen plasma system (Zepto, Diener Electronics GmbH, Germany) in conditions of 0.5 mbar for 1 min at the room temperature. Then, glass slides were left overnight. The samples were rinsed and covered with filtered seawater. Regardless of the algal cell types, the force spectroscopy was performed immediately after sample preparation.

Results

Cell growth dynamics

The growth curves of three selected algal monocultures (*D. tertiolecta*, *T. suecica*, *C. closterium*) at three growth temperatures (12 °C, 18 °C, and 30 °C) are shown in Figure S2. The data showed that growth depends on temperature conditions. The initial number of cultured cells in the growth medium was similar for all species studied, approximately 2.0×10^4 cells mL^{-1}. Table S1 summarises calculated growth rate and doubling time of three selected algae in the exponential growth phase at 12 °C, 18 °C, and 30 °C. For *D. tertiolecta* and *T. suecica*, the fastest growth and the shortest doubling time were obtained at 18 °C, which was considered a favourable temperature. For *C. closterium*, the fastest growth and the shortest doubling time were determined at 30 °C.

Motility characterisation

Qualitative insight of *D. tertiolecta* cells movement at selected temperatures is presented in Fig. 1.

At the temperature of 12 °C, about 40% of cells (69 cells) were stationary or exhibited erratic on-the-spot movement (Table S2), while the quantified trajectories of the majority of cells (101 cells) had a linearity ratio of 0.12 with an average movement time of 3.6 s. At the temperature of 18 °C, a total of 264 cells were counted in the sample, of which 21% were stationary, while 79% demonstrated random movement depicted with the broken-line type of trajectories and the linearity ratio of 0.36 during an average movement time of 2.5 s. At the temperature of 30 °C, about 22% of cells were stationary, while 78% showed similar qualitative movement to the control at 18 °C, but with a higher linearity ratio of 0.45 during an average movement time of 3.2 s.

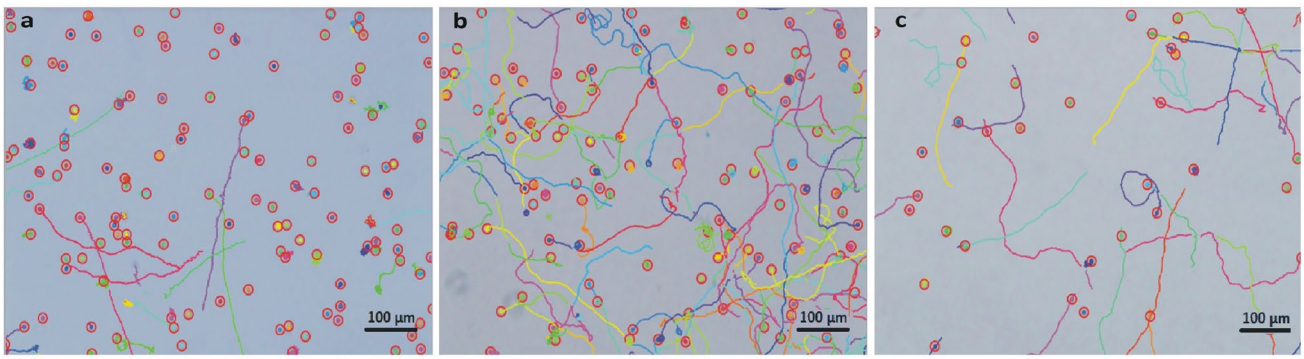

Fig. 1 Reconstructed ICY images of *D. tertiolecta* grown at temperatures of (**a**) 12 °C ($2.3x10^6$ cells mL^{-1}), (**b**) 18 °C ($5.3x10^6$ cells mL^{-1}), and (**c**) 30 °C ($1.7x10^6$ cells mL-1). Distance bar denotes 100 µm. Cells and their trajectory are denoted with coloured circles and curved coloured lines, respectively

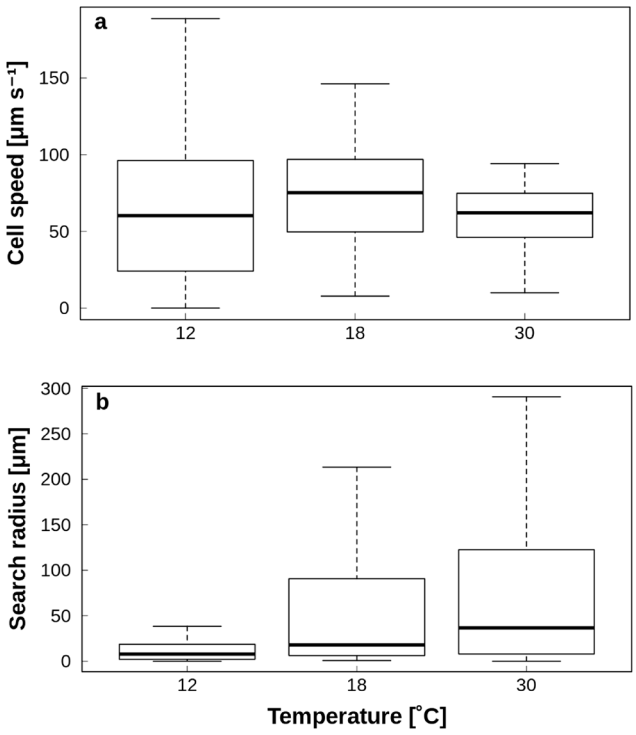

Fig. 2 Box plots of cell speed (**a**) and search radius (**b**) of *D. tertiolecta* grown at temperatures of 12 °C ($2.3x10^6$ cells mL^{-1}), 18 °C ($5.3x10^6$ cells mL^{-1}) and 30 °C ($1.7x10^6$ cells mL^{-1})

Box plots of cell speeds are presented in Fig. 2a.

The medians at 12 °C and 30 °C were almost identical. At the temperature of 12 °C, the average cell speed corresponded to 63 ± 3 µm s^{-1}, while at the 30 °C, the average speed is 62 ± 4 µm s^{-1} (Table S3). At 18 °C, cells were moving with an average speed of 72 ± 2 µm s^{-1}, which amounts to 6 body lengths per second.

From the whiskers above and below the median at 12 °C and 30 °C, it follows that the corresponding distributions of speeds deviated from the normal distribution. Indeed, the probability density distributions of cells speed (Figure S3a) revealed that all three distributions deviated from the normal distribution (for 12 °C, $\alpha_3 = 0.6$; for 18 °C, $\alpha_3 = -0.3$; for 30 °C, $\alpha_4 = 12$). The Shapiro–Wilk test confirmed that all three distributions differed significantly from the normal (for 12 °C, $W = 0.94$, $p = 9.3e\text{-}07$; for 18 °C, $W = 0.96$, $p = 1.8e\text{-}06$; and for 30 °C, $W = 0.84$, $p = 4.4e\text{-}07$). The Wilcoxon rank sum test showed that the median speed at 12 °C differed significantly from the median at 18 °C ($W = 18{,}487$, $p = 0.002$) and that the median at 30 °C differed significantly from the median at 18 °C ($W = 11{,}322$, $p = 0.0009$). However, the median at 12 °C did not differ significantly from the median at 30 °C ($W = 5707$, $p = 0.9$) as it is observable from the box plot (Fig. 2a), although the corresponding distributions are very different (Figure S3a): (a) the peak of the probability density distribution for 12 °C was close to 20 µm s^{-1}, while for 30 °C, it was close to 60 µm s^{-1}; and (b) the distribution at 12 °C resembled chi-square distribution with $k = 3$, i.e. positively skewed with a long tail, while the distribution at 30 °C was much closer to the Maxwell–Boltzmann distribution of velocities with the scaling factor of $a = 2$.

At the temperature of 12 °C, the average search radius of cells in the sample was 24 ± 4 µm. At the temperature of 18 °C, the average search radius of cells was almost doubled and was 57 ± 5 µm, while the median was only 18 µm. At the temperature of 30 °C, the average search radius increased further to 80 ± 12 µm. The box plots in Fig. 2b showed a progressive increase in the median of the search radius going from 12 °C until 30 °C. However, they also showed that with the increase in the search, radius comes a greater variation toward higher values.

The probability density distributions plot (Figure S3b) of the three samples showed that the distributions of search radius are far from normal. Indeed, Shapiro–Wilk test confirmed that the distributions are significantly different from the normal distribution (for 12 °C, $W = 0.4$, $p < 2.2e\text{-}16$; for 18 °C, $W = 0.7$, $p < 2.2e\text{-}16$; and for 30 °C, $W = 0.8$, $p = 1.503e\text{-}08$). The Wilcoxon rank sum test showed that the medians at 12 °C and 18 °C were significantly different ($W = 14{,}201$, $p = 1.051e\text{-}10$) and also that the medians at 12 °C and 30 °C were significantly different ($W = 3345.5$, p value $= 3.902e\text{-}07$). However, the test revealed that the medians at 18 °C and 30 °C were not significantly different ($W = 8054.5$, $p = 0.192$). This result arose from predominantly similar tails of the distributions but certainly not from the difference in their peaks. The peak of the probability density distribution at 18 °C was only 60% of the higher peak of the probability density distribution at 30 °C. Also, the average search radius of moving cells at 12 °C was about 40% of the value at 30 °C (Table S2).

It should be noted that the percentage of vibrating cells, i.e. cells with almost no net movement at 12 °C, was double the percentage at 30 °C (Table S2). The average speed of vibrating cells was about 40% of the speed of the moving cells. Their search radius was about 3% of the search radius of the moving cells. Examination of speed and search radius of moving cells only (Table S2) revealed that cells at 12 °C have the highest speed (87 ± 3 µm s^{-1}) versus 81 ± 2 µm s^{-1} at 18 °C and 71 ± 4 µm s^{-1} at 30 °C. Moreover, they have the smallest search radius: 40 ± 4 µm at 12 °C versus 72 ± 5 µm at 18 °C and 102 ± 12 µm at 30 °C. With a raise in temperature from 12 °C to 30 °C, the search radius increased 2.6 times.

Figure 3 provides a qualitative insight into *T. suecica* cell movement at the three selected temperatures.

In contrast to *D. tertiolecta, T. suecica* cells showed more pronounced movement. Box plots of median speed, average speed, and search radius with corresponding probability density distributions are presented in Fig. 4a and b and Figures S4a and b, respectively.

The medians of speed at 18 °C (201 µm s^{-1}) and 30 °C (194 µm s^{-1}) were similar, while the median at 12 °C was considerably smaller (113 µm s^{-1}). At the temperature of 12 °C, the average cell speed in the sample corresponded to 128 ± 14 µm s^{-1}, while the average speed at the 30 °C was 179 ± 7 µm s^{-1}. At the 18 °C, cells moved with the highest average speed of 190 ± 5 µm s^{-1} which is nearly 13 body lengths per second (Table S4a).

From the whiskers above and below the median at 12 °C and 30 °C, it can be observed that the speed distributions were not normal. The probability density distributions (Figure S3) revealed that none of the three distributions are likely to be normal (for 12 °C, $\alpha_3 = 0.4$; for 18 °C, $\alpha_3 = -0.4$; for 30 °C, $\alpha_3 = -0.1$). Indeed, the Shapiro–Wilk test confirmed that all the three distributions differed significantly from the normal (for 12 °C, $W = 0.91$, p value = 0.002; for 18 °C, $W = 0.97$, $p = 8.8e\text{-}05$; and for 30 °C, $W = 0.97$, $p = 0.004$. The Wilcoxon rank sum test showed that the median speed at 12 °C differed significantly from the median at 18 °C ($W = 3853$, $p = 3.7e\text{-}05$), but the median at the 18 °C did not differ significantly from the median at 30 °C ($W = 20{,}366$, $p = 0.19$). Finally, the median at 12 °C differed significantly from the median at 30 °C ($W = 2411$, $p = 0.001$), as shown on the box plot.

The negatively skewed probability density distributions at 18 °C and 30 °C did not differ significantly and their peak was at about 240 µm s^{-1} (Figure S4a), as was confirmed by the Wilcoxon's test. The positively skewed probability density distribution of speeds at 12 °C had two peaks, the dominant one at about 50 µm s^{-1} and the inferior one at approximately 230 µm s^{-1}.

Box plots of cells' search radii in the sample at the three temperatures are presented in Fig. 4b. The medians of the search radius at 12 °C (16 µm) and 30 °C (31 µm) are closer to each other than the median at 18 °C, which is from 3 to 6 times larger (102 µm). At the temperature of 12 °C, the average cell search radius of the sample

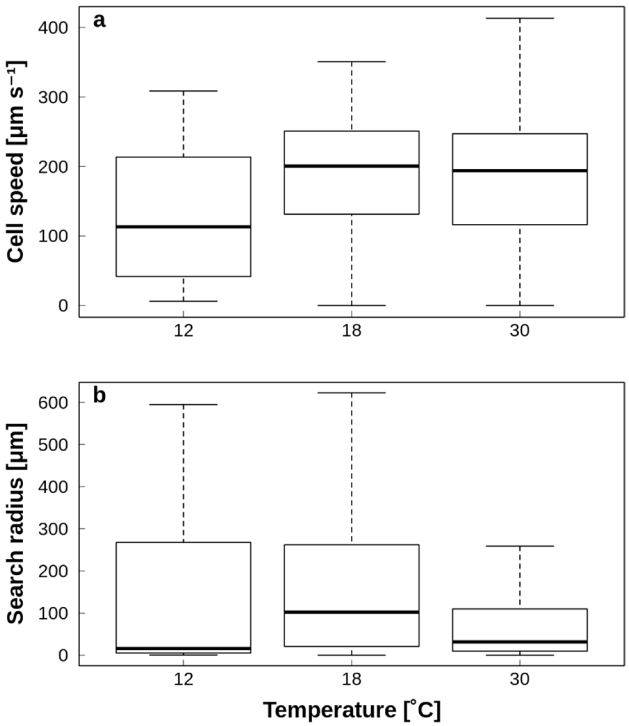

Fig. 4 Box plots of cell speed (**a**) and search radius (**b**) of *T. suecica* grown at temperatures of 12 °C (2.3x10^5 cells mL^{-1}), 18 °C (1.9x10^6 cells mL^{-1}) and 30 °C (9.4x10^5 cells mL^{-1})

corresponded to 127 ± 26 µm, while at the 30 °C the average speed was 80 ± 9 µm (Table S4a, b). At the 18 °C, the average search radius of *T. suecica* was 163 ± 11 µm which amounted to about 12 body lengths.

As noted from the whiskers above and below the median at all tested temperatures and from Figure S4b, all three distributions were positively skewed and far from a normal distribution. Indeed, the Shapiro–Wilk test confirmed that all three distributions differ significantly from the normal (for 12 °C, $W = 0.73$, p value = 5.5e-08; for 18 °C, $W = 0.84$,

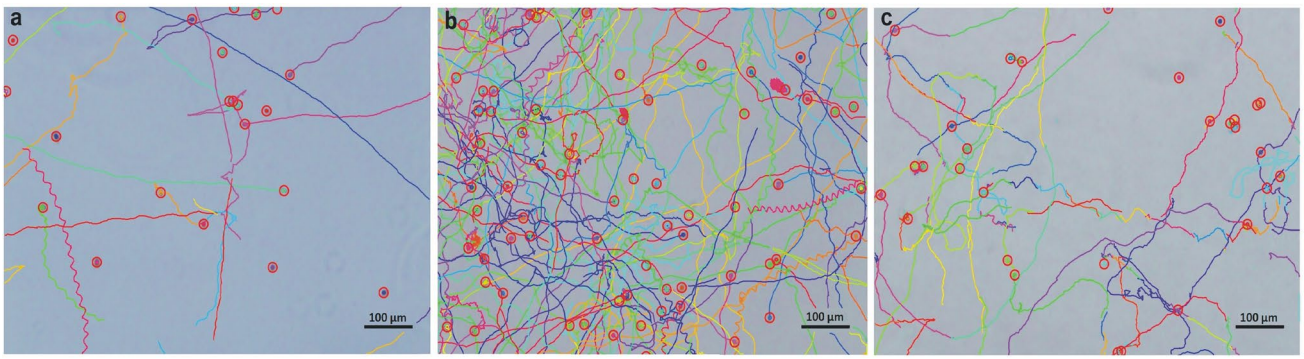

Fig. 3 Reconstructed ICY images of *T. suecica* grown at temperatures of (**a**) 12 °C (2.3x10^5 cells mL^{-1}), (**b**) 18 °C (1.9x10^6 cells mL^{-1}), and (c) 30 °C (9.4x10^5 cells mL^{-1}). Distance bar denotes 100 µm. Cells and their trajectory are denoted with coloured circles and curved coloured lines, respectively

$p = 1.4e\text{-}15$; and for 30 °C, $W = 0.73$, $p = 3.4e\text{-}15$). The Wilcoxon rank sum verified that the median of search radius at 12 °C differed significantly from the median at 18 °C ($W = 4561$, $p = 0.004$). In addition, the median at the 30 °C differed significantly from the median at 18 °C ($W = 24{,}953$, $p = 7.9e\text{-}08$), but the median at 12 °C did not differ significantly from the median at 30 °C ($W = 3377.5$, $p = 0.66$), as it was shown on the box plot.

The positively skewed probability density distributions showed that the search radius and the speed of cells were increasing from 12 to 18 °C. On the other hand, the average search radius at 30 °C was the smallest, although the average speed of cells was the highest. This showed that the linearity of movement was much lower, i.e. the cells wiggled much more than at progressively smaller temperatures.

Electrochemical characterisation of algal cells and released surface-active matter

Electrochemical adhesion-based characterisation of isolated algal cells resuspended in seawater was performed by recording polarograms of oxygen reductions. The polarogram recorded in the *D. tertiolecta* cell suspension showed the appearance of irregular perturbations in the defined potential, resulting from the cell adhesion at the charged interface (Fig. 5a).

No perturbations were recorded outside of this potential range (more positive and negative), indicating that cell adhesion is not present. The polarograms recorded in the cell suspensions of *T. suecica* and *C. closterium* were perfectly regular, without the occurrence of perturbations, i.e. these cells behaved as inert and no adhesion takes place. Therefore, only the cells of *D. tertiolecta* were used to test the effect of temperature on cell adhesion behaviour at the wide potential range. The dependence of the amperometric signal frequency on applied potentials at three temperatures in *D. tertiolecta* suspensions with similar cell densities is shown in Fig. 5b. The narrowest potential range of adhesion was recorded in the *D. tertiolecta* cell culture grown at 12 °C, denoted by critical potentials of –192 mV and –1200 mV in seawater. The most negative and the most positive potential in which at least one amperometric signal per 10 consecutive I–t curves appears corresponded to critical potentials (Ec^+, Ec^-, Žutić et al. 1993; Ivošević et al. 1994). For the cell suspension grown at the 30 °C, the measured critical potentials of adhesion corresponded to −184 and −1170 mV, while the broadest potential range of cell adhesion was recorded in the cell suspension grown at the temperature of 18 °C, from −110 to −1240 mV, which offers a favourable growth condition for the corresponding cell. The lowest number of amperometric signals of cells was recorded in cell suspension grown at 12 °C. The number of recorded amperometric signals increased with the increase in temperature used in cell culture. The maximum number of amperometric signals occurred at the potential of –400 mV at all three examined temperatures, since interfacial tension is close to the maximum value (electrocapillary maximum). At this potential, the mercury electrode is positively charged and electrostatic attraction prevails in between the positively charged interface and the negatively charged *D. tertiolecta* cells. By shifting the potential either positively or negatively from –400 mV, interfacial energy decreases, and the number of amperometric signals of the cells decreases accordingly. On the other hand, at the potential of −800 mV, the mercury electrode is negatively charged, and signal frequency is lower due to the electrostatic repulsion with the negatively charged *D. tertiolecta* cells.

Quantitative characterisation of the released surface-active matter in the growth medium was determined by recording polarograms of Hg(II). The polarographic maximum of Hg(II) is sensitive for the adsorption of dissolved organic matter and submicron particles, which is manifested cumulatively as a gradual decrease in the reduction current proportional to surfactant concentration in the sample. Surfactant activity at different growth temperatures was determined and expressed per cell (Fig. 5c). The data showed that surfactant activity is the highest in *C. closterium* at 12 °C, then in *D. tertiolecta* at 30 °C, while the lowest surfactant activity is determined in *T. suecica* cells.

Nanoscale imaging of algal cell and released extracellular biopolymers

Morphological characterisation of *D. tertiolecta, T. suecica*, and *C. closterium* cells at 12 °C, 18 °C, and 30 °C was performed by AFM. The representative images of individual algal cells for each species are shown in Fig. 6.

All three species maintained the same overall cell shape regardless of the temperature, with no nanostructural changes observed on the cell surface. The cells of *D. tertiolecta* had an ovoid shape with two flexible flagella that were distinguishable from the cell body (Fig. 6a). The cell body length was in the range of 7.5–12.1 µm, and the cell width was 4.5–6.8 µm. Flagella had a length of 17–20 µm and a height of 90 nm. The cells of *T. suecica* had an ellipsoid shape with four flexible flagella that were distinguishable from the cell body (Fig. 6b). The cell body length was in the range 14.0–20.1 µm and cell width 8.5–14.7 µm. The flagella had a length of 8.7–10.2 µm and a height of about 200 nm. Granular structures observed on the surface of *T. suecica* probably correspond to micropearls previously identified by SEM (Martignier et al. 2018), thus

being the first AFM-based observation of micropearls in the genus *Tetraselmis*.

Cylindrotheca closterium cells possessed an elongated shape with flexible rostrae that could be clearly distinguished from the central part of the cell (Fig. 6c). The cell body length was in the range 30.5–60.2 µm, and cell width was 2.8–8 µm. Three morphologically different parts of the frustule could be distinguished: the girdle band, the valve, and the raphe. The longitudinal slit raphe extends along with the valve and is bridged by the fibulae. The spacing between fibulae was 250–350 nm, and fibulae arches underneath the cell wall were noticeable. High-resolution images of the central part of the cell revealed a non-structured and smooth surface of the valve, whereas the girdle band showed a structured surface consisting of a set of parallel bands. Morphological parameters including cell length, cell width, cell height, and cell surface roughness of the cells grown at different temperatures based on AFM image analysis are summarised in Table S5. The length, width, and height of *D. tertiolecta* grown at 12 °C and 18 °C were similar. However, the cells grown at 30 °C were smaller in both length and width, but with a maintained cell height. The roughness of *D. tertiolecta* cell surface was in a similar range for all temperatures. The length, width, and height of *T. suecica* grown at 12 °C and 18 °C were similar, while cells grown at 30 °C were smaller in both length and width and with no change in cell height. The roughness of *T. suecica* cell surface grown at different temperatures was in a similar range. The size (length, width, and height) of *C. closterium* had the highest values at 12 °C. The length, width, and height of *C. closterium* grown at 18 °C and 30 °C were similar. The roughness of *C. closterium* valve and girdle increased accordingly with the increase in temperature.

Supramolecular organisation of released materials of *C. closterium, D. tertiolecta*, and *T. suecica* at temperatures of 12 °C, 18 °C, and 30 °C were imaged (Fig. 7).

The extracellular polymer substance (EPS) of *C. closterium* formed a network of fibrils at all examined temperatures. The EPS of *C. closterium* grown at 12 °C was located all around the cell and the network appeared denser (Fig. 7a). The height range of fibrils was in the range of 1.5–4 nm. At temperatures of 18 °C and 30 °C, the released EPS fibrils were mostly located around the apices of rostra with a height range of 1–4 nm (Fig. 7b, c). The released material was visible around *D. tertiolecta* cells (Fig. 7d) grown at 12 °C and consisted of the fibrillar network (height 0.7–1.5 nm) with incorporated globules (height 2.5–10 nm). At the temperatures of 18 °C and 30 °C, only aggregated particles (height 2–5 nm) were observed around *D. tertiolecta* cells (Fig. 7e). Although fixation could introduce artefacts, the relative change in the organisation of released polymers from *D. tertiolecta* cells was distinguished. At selected temperatures, only aggregated particles with a height range of 5–25 nm were observed around the cells of *T. suecica* (Fig. 7f).

Nanomechanical characterisation of algal cells by AFM

An individual algal cell was localised on the substrate using an inverted optical microscope (Fig. 8a). Force curves were recorded at the central area of the cell body within a scan area of 3×3 µm. Representative maps of local elastic (Young's modulus, *E*) and adhesive properties (maximum work of adhesion, W_{adh}) of the *D. tertiolecta* cell are shown in Fig. 8c and d, respectively.

The overlay of the box-plots and Young's modulus distributions obtained for *D. tertiolecta*, *T. suecica*, and *C. closterium* cells cultured at 12 °C, 18 °C, and 30 °C are presented in Fig. 9.

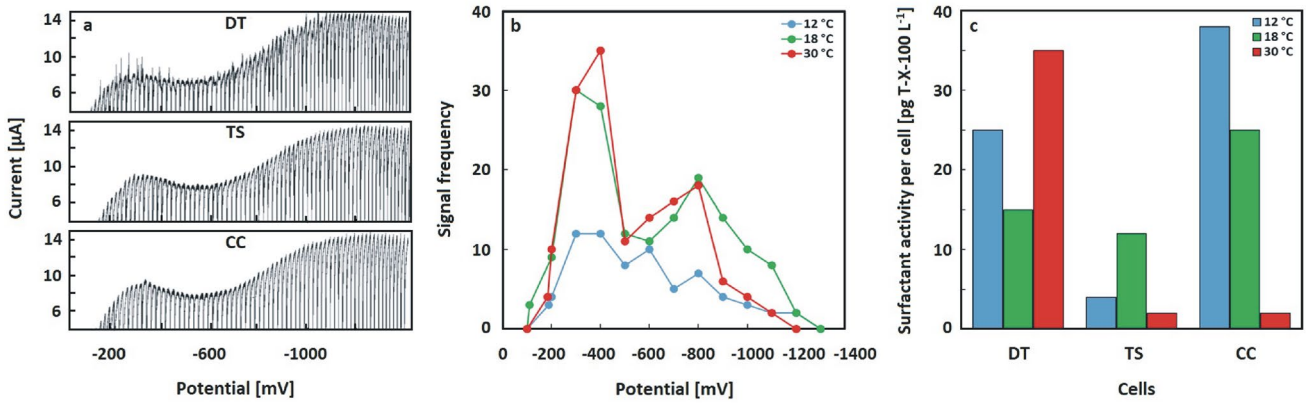

Fig. 5 Polarograms of oxygen reduction recorded in *D. tertiolecta, T. suecica* and *C. closterium* cell suspensions in seawater (**a**); potential dependence of the signal frequency of *D. tertiolecta* cells grown at temperatures of 12 °C, 18 °C, and 30 °C (**b**) and surfactant activity for examined cell species at selected temperatures (**c**)

Regardless of the temperature conditions, *D. tertiolecta* cells are characterised by the lowest Young's modulus ranging from a few to 40 kPa. *T. suecica* cells are stiffer with the *E* varying from 1 to 300 kPa. For *C. closterium*, the *E* values varied even within one single cell from kPa to MPa. Considering that Young's moduli distributions are broad and non-symmetric, we have compared median values among the studied cell populations. The median was accompanied by an interquartile range (*Q3-Q1*), which describes where the central 50% of data lie.

The mechanical properties of algal cells were dependent on the temperature (Fig. 9). We found that *D. tertiolecta* cells stiffen at low temperature (a median of the Young's modulus is equaled to 6.4 kPa (*Q3-Q1* = 9.1 kPa)) at 12 °C and become more compliant at higher temperatures, i.e. 3.5 kPa (*Q3-Q1* = 3.2 kPa) at 18 °C and 1.5 kPa (*Q3-Q1* = 4.6 kPa) at 30 °C. The statistical significance for all groups was below 0.0001 for the 0.05 significance level (Kruskal–Wallis ANOVA test). Median (*Q3-Q1*) values determined for *T. suecica* at 12 °C, 18 °C, and 30 °C were 42.8 kPa (75 kPa), 45.9 kPa (80.2 kPa), and 44.7 kPa (65.7 kPa), respectively. Data sets for algal cells cultured at 12 °C and 18 °C and algal cells cultured at 18 °C and 30 °C showed a statistical significance ($p < 0.05$ for all data groups). No statistical difference was observed for 12 °C and 30 °C. *C. closterium* cells are characterised by the largest modulus distributions. Despite that, analogously to *T. suecica*, a statistical significance ($p < 0.05$) was noted among the groups of algal cells cultured at various temperatures. The corresponding medians (*Q3-Q1*) were 292 kPa (332 kPa), 214 kPa (436 kPa), and 152 kPa (577 kPa).

Adhesive and hydrophobic properties of algal cells

The change in the hydrophobic properties (ΔW_{adh}) of the algal cell surface is quantified from the subtraction of the work of adhesion determined for bare and OTS-coated cantilevers (Fig. 10a, b; expression 6).

The positive value of ΔW_{adh} denotes the domination of hydrophilic interactions, while its negative values indicate that the hydrophilicity is smothered by the hydrophobicity. Table S6 presents the mean value of the maximum work of adhesion (± standard error of the mean, *SEM*) obtained from measurements with bare and OTS-coated cantilevers. The relative probability of adhesion (*P*) between each studied cell line with the bare and CH_3-functionalised silicon nitride AFM probe is presented in Figure S5. The results obtained from the maximum work of adhesion, as well as adhesion probability, showed species-specific and temperature-dependent changes. In the case of *D. tertiolecta* cells, the probe modification resulted in a slight decrease in adhesion probability regardless of temperature conditions. A contrasting trend was observed for *T. suecica* cells cultured at 18 °C and 30 °C, where probe modification significantly diminished adhesion probability. Interestingly, this was not the case for cells cultured at 12 °C, for which the probability of adhesion increased from 31 to 47%. A similar observation referred to *C. closterium* cells cultured at 12 and 30 °C. When probed with an OTS-modified tip, *P* value increased from 2 to 13% and from 42 to 55%, respectively. At 18 °C, the probability of adhesion between a bare probe and *C. closterium* cell was higher than between an OTS-modified tip and the cell.

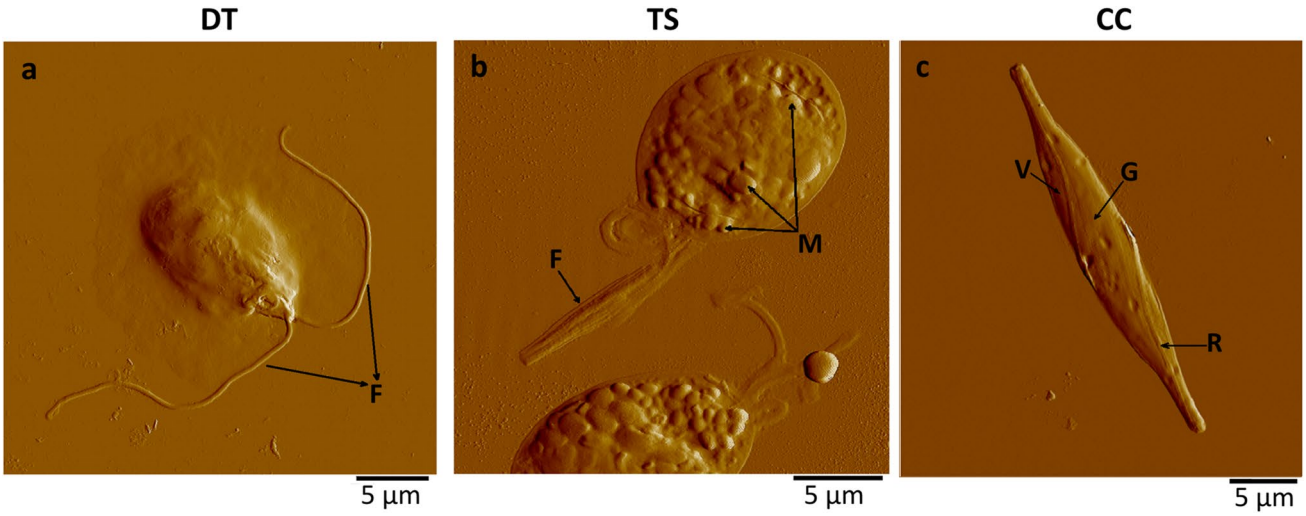

Fig. 6 AFM deflection images of *D. tertiolecta* (**a**), *T. suecica* (**b**) and *C. closterium* (**c**) cells. Images are acquired using contact mode in the air with scan sizes: 30x30 µm (**a**) 25x25 µm (**b**) and 40x40 µm (**c**). Letters F, M, V, G and R indicate the following features: flagellae, micropearls, valve, girdle band, and raphe opening, respectively

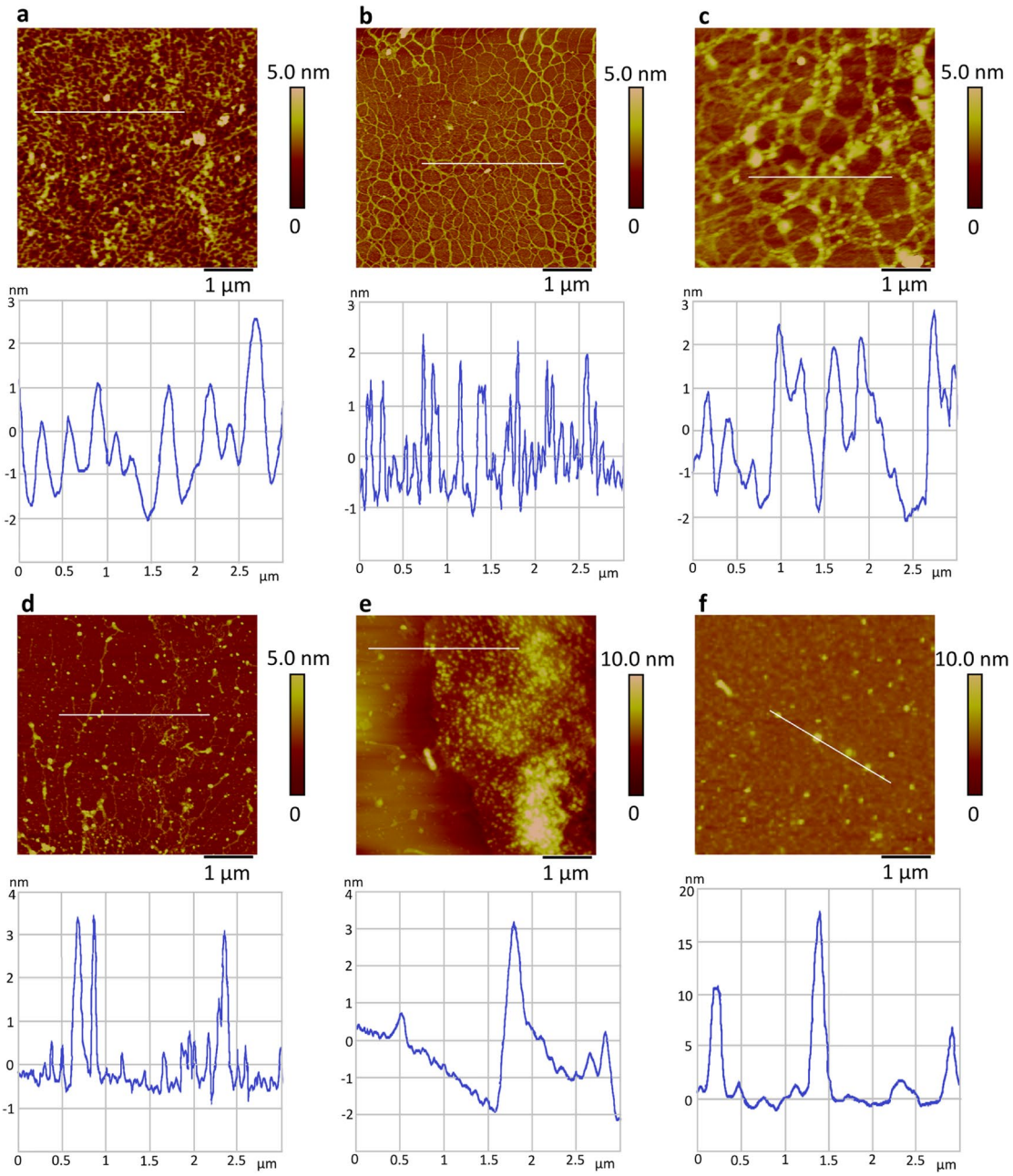

Fig. 7 AFM topographical images of extracellular polymers of *C. closterium* grown at 12 °C (**a**), 18 °C (**b**) and 30 °C (**c**). *D. tertiolecta* grown at 12 °C (d) and 18 °C (e); *T. suecica* grown at 18 °C (f); Images are acquired using contact mode in air and presented as height data with vertical profiles along indicated lines. Scan sizes: 5x5 µm

The balance between the hydrophobic and hydrophilic properties of algal cells is depicted in Fig. 10c. The first observable showed variability among the studied algal cells and temperature. Starting from 12 °C, the surface of *D. tertiolecta* and *T. suecica* cells demonstrated hydrophilic character, while the surface of *C. closterium* seems to be more hydrophobic. The relation between surface properties of algal cells extending from hydrophilic to hydrophobic can be expressed as *D. tertiolecta* > *T. suecica* > *C. closterium*, respectively. The increase to 18 °C caused an abrupt change in the surface properties, with the cells of *C. closterium* possessing the most hydrophilic surface. A similar degree of surface hydrophilicity present on the cells of *D. tertiolecta* and *T. suecica* was outlined by extremely low values of ΔW_{adh}, i.e. 0.0094 ± 0.0018 fJ and 0.0063 ± 0.0028 fJ, respectively. However, the overall net surface properties

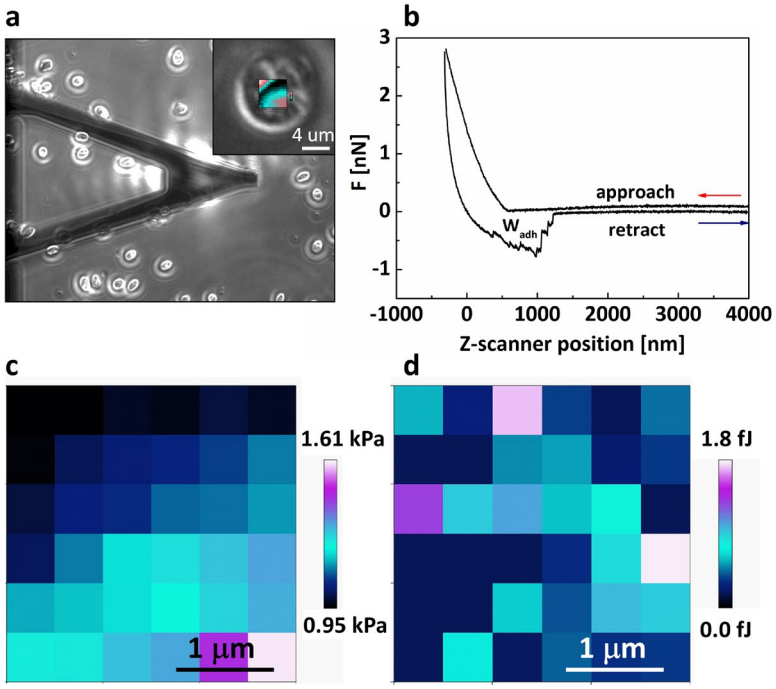

Fig. 8 Phase-contrast microscopic image of the bare MLCT-D cantilever and *D. tertiolecta* cells cultured at 30 °C (**a**). An example of the corresponding force curve recorded on a single *D. tertiolecta* cell (**b**). Representative maps of local elastic (Young's modulus, (**c**)) and adhesive properties (maximum work of adhesion (**d**))

were still hydrophilic. Further increase to 30 °C changed the relationship between the surface properties of algal cells once more.

The surface of *D. tertiolecta* and *T. suecica* cells was characterised by high $W_{adh\ (no\ OTS)}$ and low $W_{adh\ (OTS)}$ values ending in a similar level of hydrophilicity. For *D. tertiolecta* cells, this value reached the level observed for 12 °C, while a much higher hydrophilicity level was observed for *T. suecica* cells. The high negative value of ΔW_{adh} obtained for *C. closterium* cells (-0.77 ± 0.08 fJ) indicates that algal cells become strongly hydrophobic at 30 °C.

Discussion

The possible ecological implications of temperature as a physical stressor on the fate of microalgae in aquatic systems are still inadequately understood. To the best of our knowledge, the effect of temperature on the surface properties and behaviour of selected microalgae has not been reported. In this study, we related temperature changes to algal response, taking into account their structural characteristics that may contribute to temperature tolerance. A summary of relationships between cell morphological characteristics and the studied parameters determined at 12 °C, 18 °C, and 30 °C, respectively, are given in Table 1.

The results showed that algal species successfully adapt to all tested temperatures. The favourable growth temperature (T_f) for *D. tertiolecta* and *T. suecica* was 18 °C, whilst it was 30 °C for *C. closterium*, which is congruent to the natural habitat conditions that the species occupy. Slow growth rates were determined when algal species were cultured at $T \neq T_f$.

Behavioural responses of algal species were analysed in terms of motility, adhesion at the charged electrode, and physiological activity. Motility analysis of flagellated species provides an insight into the physiological state of algal cells in culture. Both *D. tertiolecta* and *T. suecica* showed pronounced motility ranging from 6 to 13 body lengths per second (cell lengths approximately 6–12 µm, respectively). Algal cell speed depends on the number of flagella that a cell possesses; thus, *T. suecica* is about 3 times faster than *D. tertiolecta* at T_f. At lower temperature ($T<T_f$), *D. tertiolecta* and *T. suecica* responded with significantly slower cell speeds and erratic movements around the spot. At higher temperature ($T>T_f$), *D. tertiolecta* and *T. suecica* responded without a significant change in cell speeds, while the search path increased with a greater variation for *D. tertiolecta*. Change in the motility behaviour of *D. tertiolecta* is probably related to change in cell stiffness and physiological activity. Mayali et al. (2008) reported that marine bacteria caused a decrease in the speed of motile phytoplankton through the release of enzymes, which could provide plausible justification of our results.

Electrochemical adhesion-based detection of algae depends on the collective surface properties (fluidity, hydrophobicity, cell surface charge) of the cell exterior. Only soft and deformable species like *D. tertiolecta* adhere to charged fluid interface in the well-defined potential range. At $T<T_f$,

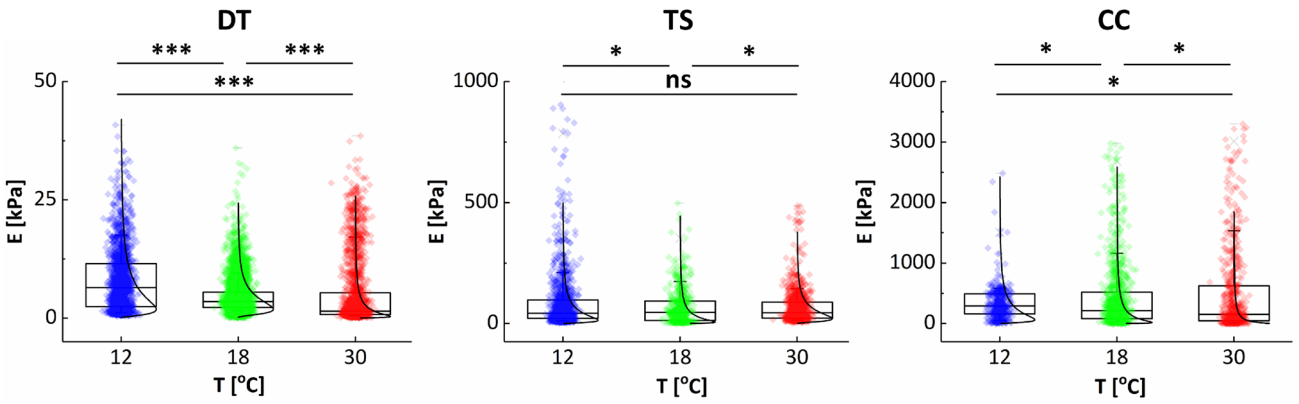

Fig. 9 Overlay of the box plots with Young's modulus distributions, obtained for *D. tertiolecta* (**a**), *T. suecica* (**b**), and *C. closterium* (**c**) cells cultured at 12 °C, 18 °C and 30 °C, were fitted with the log normal function (black line). A box with whiskers represents a median ± interquartile range (Q3-Q1). Statistical significance was obtained from Kruskal-Wallis ANOVA test at the level of 0.05 (*** $p < 0.0001$, ns – not statistically significant)

the potential range of adhesion is the narrowest, due to determined stiffness and a distinct physiological activity of *D. tertiolecta*. The adhesion efficiency of *D. tertiolecta* is the lowest at $T<T_f$ due to the competitive adsorption of released organic material which masks single cell adhesion (Ivošević and Žutić 1997; Kovač et al. 1999). At T_f, the cells of *D. tertiolecta* adhered in the broadest range designated with the critical potentials from −110 to −1240 mV. The adhesion of *D. tertiolecta* cells exists within a wide range of surface charge density, where the electrode carries positive and negative polarities, thus showing the predominance of hydrophobic over electrostatic interactions in the adhesion process (Svetličić et al. 2001). The high probability (over 75%) of adhesion between an AFM probe and *D. tertiolecta* cells also supports this conclusion (Figure S5). The manifestation of electrostatic interactions between the negatively charged cell and the negatively charged electrode is detected through lower signal frequency and critical interfacial tension of adhesion. The critical interfacial tensions can be determined from the critical potentials and electrocapillary data for an aqueous electrolyte solution. Since electrocapillary data for natural seawater is not available, the reported critical interfacial tensions for adhesion of *D. tertiolecta* at mercury/0.1 M NaCl showed to be different at the positively and negatively charged interface probably due to the electrostatic repulsion (Svetličić et al. 2001; Novosel and Ivošević

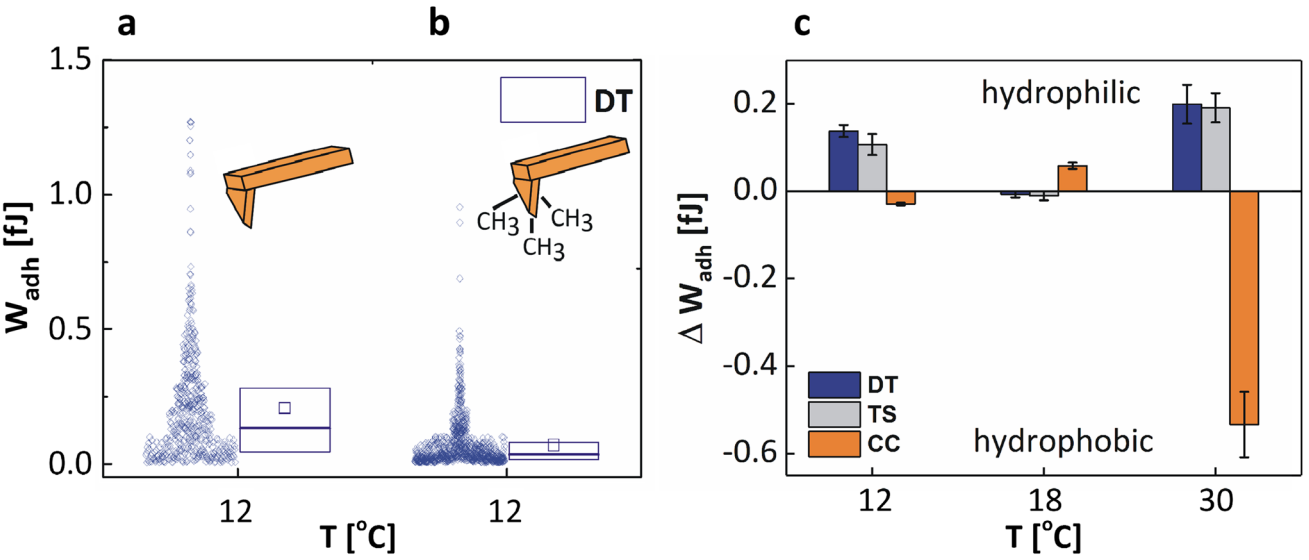

Fig. 10 Exemplary distribution of maximum work of adhesion obtained for *D. tertiolecta* cells cultured at 12 °C and probed with a bare silicon nitride ($W_{adh\ (no\ OTS)}$, **a**) and CH_3–modified (hydrophobic) AFM cantilevers ($W_{adh\ (OTS)}$, **b**). The balance between hydrophilic and hydrophobic properties of algal cell surface plotted for 12 °C, 18 °C, and 30 °C (data are presented as $\Delta W_{adh} \pm$ maximum error, **c**)

DeNardis 2021). In contrast, the adhesion and spreading of *T. suecica* and *C. closterium*, which are stiffer by 2–3 orders of magnitude, are hindered by the mechanical strength of the cells; therefore, these species were not detected at the fluid interface. The mechanical properties of cells are related to fatty acid composition and content. Low content of polyunsaturated fatty acids (PUFAs) was present in diatoms (Barreira et al. 2015), as opposed to the very high content of PUFAs (higher than 50% of total fatty acids, FAs), which are commonly found in green algae (most notably in *D. tertiolecta* and to some less extent in *T. suecica*).

Physiological activity of the cells, expressed as electrochemically measured surfactant activity, refers to released organic material, which appears to be species-specific and temperature-dependent. The most pronounced surfactant activities were determined at 12 °C for *C. closterium* and at 12 °C and 30 °C for *D. tertiolecta*, which were shown to be unfavourable to cell growth. The lowest amount of released organic material is determined for *T. suecica* regardless of the temperature (Fig. 5c).

Our results show differences in the supramolecular organisation of extracellular polymeric substances in the selected species as a function of temperature change. The structural organisation of the released organic material probed by AFM revealed the form of a polysaccharide-rich EPS network around the entire cells of *C. closterium.* Since the corresponding cells cannot easily escape, they must cope with environmental changes by altering their cellular metabolism through considerable physiological activity (Hader et al. 2015). Physiologically, cells secrete an excessive amount of structurally and compositionally diverse biopolymers, mainly consisting of polysaccharides, proteins, nucleic acids, and lipids. The microalgal EPS is acidic, negatively charged and somewhat hydrophobic due to the anionic components of the polysaccharide chains, such as acetyl groups, uronic acids and sulphates, which are important for its adhesive properties (Bertocchi et al. 1990; Dade et al. 1990; Mata et al. 2006; Urbani et al. 2005; Mishra et al. 2011). The EPS of *C. closterium* and *D. tertiolecta* was organised in the form of dense fibrils or globular structures. *T. suecica* was characterised by the lowest release of extracellular material, regardless of temperature, with no effect on the material organisation. Both surface methods concurred that a pronounced extracellular release was observed in *C. closterium*. Wolfstein et al. (2002) reported that the highest amounts of EPS were produced at 15 °C and 25 °C during the early stationary growth phase of diatoms. When EPS concentrations were normalised to chlorophyll *a*, maximum values were measured at 4 °C and 10 °C, which is consistent with our results.

The detailed AFM characterisation of algal surface morphology showed no specific change under temperature variation, but the change was detected in the size of algal species. The cells of *T. suecica* and *D. tertiolecta* were smallest at 30 °C. However, the cells of *C. closterium* grown at 18 °C and 30 °C were similar in size, but smaller compared to cells grown at 12 °C. Temperature-induced change in cell size probably indicates cytoskeletal rearrangements. An inverse relationship between cell size and temperature, known as the temperature-size rule, is commonly observed in eukaryotes (Atkinson et al. 2003). At higher temperatures, the reduced organism size corresponds to an adaptive plastic response

Table 1 Relationship between morphology and studied parameters examined at 12 °C and 30 °C versus 18 °C

Temperature & Parameters	Morphology		
	Biflagellated naked cell	Tetraflagellated cell with calcite incrusted theca	Gliding cell with organosilicate cell wall
12 °C			
Growth rate	Lowest	Lowest	Lowest
Cell size	No change	No change	Increase
Cell speed	Low	Lowest	n.a
Adhesion efficiency	Lowest	n.a	n.a
Physiological activity	High	Low	Highest
Stiffness	Highest	No change	Highest
Hydrophobicity	Hydrophilic	Hydrophilic	Hydrophobic
30 °C			
Growth rate	High	High	Highest
Cell size	Increase	Increase	No change
Cell speed	Lowest	Low	No change
Adhesion efficiency	Highest	n.d	n.d
Physiological activity	Highest	Lowest	Lowest
Stiffness	Lowest	No change	Lowest
Hydrophobicity	Highest hydrophilicity	Highest hydrophilicity	Highest hydrophobicity

resulting from earlier reproduction as the population growth rate increases, as well as accelerated completion of the life cycle at the expense of maturation size.

Furthermore, AFM measurements revealed that the surface properties of algal cells were both species-specific and temperature-dependent and can be linked to the structural features of the algal cell lines. *D. tertiolecta* does not possess a cell wall, while *T. suecica* is embedded in a thin calcite-encrusted theca. Temperature had the strongest impact on *D. tertiolecta*, exerting both mechanical and chemical changes. Increasing temperature caused a decrease in the stiffness of *D. tertiolecta*, in addition to changes in the degree of hydrophilicity. Correspondingly, the cells of *C. closterium* became softer at $T>T_f$ and temperature triggered a chemical change, so cells become hydrophobic, suggesting a molecular modification of the cell wall. Besides the change in the cells, their main secretion products were mainly characterised as hydrophilic in the early growing phase, whilst the later phase was characterised by predominantly hydrophobic compounds (Ciglenečki et al. 2018). Our previous study revealed heterogeneity within the elasticity maps of *C. closterium*, with the valve appearing softer (29.8 MPa) than the girdle region (43.7 MPa on silica strips and 21.3 MPa between the strips, respectively). The obtained results suggest that the valve has a lower silica content and is enriched with organic material (Pletikapić et al. 2012). In the case of *T. suecica* cells, the temperature-dependent direction of these changes cannot be defined. A very low level of hydrophilicity observed at 18 °C, increases with the temperature change. Also, *T. suecica* cells are softer at 12 °C and 30 °C ($T \neq T_f$), as opposed to the stiffer cells at 18 °C. The probability of adhesion is determined to be similar whether *D. tertiolecta* adheres to a bare or OTS-modified cantilever, which is in line with electrochemical-adhesion based study of *D. tertiolecta* in the wide potential range (Fig. 5b). In addition, more pronounced differences are found in the adhesion probability obtained for the other two algae adhering to a hydrophilic and hydrophobic AFM probe (Figure S5).

We demonstrated that the physicochemical properties of the biointerface provide a detectable species-specific and temperature-dependent change in the adaptive response of algal cells. Differences in the adaptive response of cells on temperature alterations can be understood through the difference in the underlying mechanisms. The algal response includes changes in the fatty acids composition through changes in hydrocarbon length, degree of saturation, charge, and headgroup of phospholipids (de Carvalho & Caramujo 2018). The ratio of PUFAs to saturated fatty acids (SFAs) determines the response of the cell membrane to exerted stress, as short-chain SFAs form less-viscous membranes, whereas PUFAs form more fluid membranes. During temperature variation, most algal cells employ several primary mechanisms for membrane stabilisation (Barati et al. 2019), which include the enhanced production of membrane unsaturated FA to decrease the membrane lipid solidification at low temperatures (Lyon and Mock 2014) or intensified synthesis and binding of saturated FA into membrane lipids and the activation of membrane-stabilising proteins (Los et al. 2013). Moreover, high temperature triggers the expression of membrane-bound heat-shock proteins that regulate protein homeostasis (Katz et al. 2007; Fulda et al. 2010) and contribute to the molecular protection and repair of membrane proteins (Ritossa 1996; Kobiyama et al. 2010; Guo et al. 2015). The fact that *T. suecica* cells do not respond similarly to temperature changes as *D. tertiolecta* and *C. closterium* could arise from differences in the ratio of membrane FAs that could be responsible for maintaining higher membrane stability and greater thermal protection (de Carvalho and Caramujo 2018).

On a fundamental level, our findings can contribute to a better understanding of the mechanism of diatom aggregation in the marine environment. *Cylindrotheca closterium* is a diatom species capable of forming benthic biofilms, as well as resuspending from the benthos and forming aggregates during bloom in aquatic systems (Wolfstein et al. 2002). Diatom aggregates are a primary source of marine snow (Thornton 2002), a ubiquitous feature of the ocean and an important means of transporting energy and nutrients in marine ecosystems. The initially hydrophilic cells of *C. closterium* only become hydrophobic when a significant increase in abundance is achieved, for which the trigger is a temperature increase. The rise in temperature promotes faster reproduction with a consequent reduction in cell size, with a concomitant decrease in EPS production and an increase in EPS hydrophobicity. At higher temperatures, the hydrophobic properties of the EPS of *C. closterium* suggest metabolic changes that enable cells to cope with challenging conditions of climate change-induced warming. The feedback generated stimulates a further diatom bloom and increases the aggregation potential of cells, thus promoting the development of marine snow and the consequent flow of nutrients through the water column (Riebesell 1991; Thornton 2002).

Conclusion

Our study showed that the surface properties and behaviour of algal cells exhibit detectable, species-specific, and temperature-dependent changes that can be related to the structural properties of the cell envelope. The most sensitive to temperature changes is the wall-less alga *D. tertiolecta*, as it exhibits the greatest mechanical and chemical changes. All cells stiffen at lower temperatures and become more compliant at higher temperatures, indicating a molecular change in the cell envelope. The increase in temperature causes an imbalance in cell hydrophobicity. *D. tertiolecta*

and *T. suecica* showed a highly hydrophilic character, while *C. closterium* became the most hydrophobic, which is of ecological importance for understanding the mechanism of algal biofilm formation. Furthermore, temperature induces a change in physiological activity in terms of concentration and structural organisation of released extracellular polymers, ranging from fibrils to dense networks. The change in cell surface properties and physiological activity is reflected in motility and adhesion behaviour at the interface. All selected algal cells maintained their overall shape without nanostructural changes at the surface. This study demonstrated that temperature-dependent surface properties and behaviour provide important evidence for understanding the adaptive mechanism of algae at the single cell level, which can be used to indicate ecosystem disturbance, algal bloom, as well as finding adequate commercial application.

Supplementary Information The online version contains supplementary material available at https://doi.org/10.1007/s10811-021-02591-0.

Funding This work is supported by the Croatian Science Foundation Project "From algal cell surface properties to stress markers for aquatic ecosystems" (IP-2018–01-5840).

Data availability The datasets generated during the current study are available from the corresponding author on reasonable request.

References

Ahmad S, Kothari R, Shankarayan R, Tyagi VV (2020) Temperature dependent morphological changes on algal growth and cell surface with dairy industry wastewater: an experimental investigation. 3 Biotech 10:24

Atkinson D, Ciotti BJ, Montagnes DJS (2003) Protists decrease in size linearly with temperature: ca. 2.5% degrees C-1. Proc Roy Soc B 270:2605–2611

Barati B, Gan SY, Lim PE, Beardall J, Phang S-M (2019) Green algal molecular responses to temperature stress. Acta Physiol Plant 41:26

Barreira L, Pereira H, Gangadhar KN, Custódio L, Varela J (2015) Medicinal effects of microalgae-derived fatty acids. In: Kim S-K (ed) Handbook of Marine Microalgae. Academic Press, Boston, pp 209–231

Beaugrand G (2005) Monitoring pelagic ecosystems using plankton indicators. ICES J Mar Sci 62:333–338

Bertocchi C, Navarini L, Cesàro A, Anastasio M (1990) Polysaccharides from cyanobacteria. Carbohydr Polym 12:127–153

Boyce DG, Lewis MR, Worm B (2010) Global phytoplankton decline over the past century. Nature 466:591–599

Ciglenečki I, Dautović J, Cvitešić A, Pletikapić G (2018) Production of surface active organic material and reduced sulfur species during the growth of marine diatom *Cylindrotheca closterium*. Croat Chem Acta 4:455–461

Dade WB, Davis JD, Nichols PD, Nowell ARM, Thistle D, Trexler MB, White DC (1990) Effects of bacterial exopolymer adhesion on the entrainment of sand. Geomicrobiol J 8:1–16

De Carvalho CCCR, Caramujo MJ (2018) The various roles of fatty acids. Molecules 23:2583–2619

Decho AW, Gutierrez T (2017) Microbial extracellular polymeric substances (EPSs) in ocean systems. Front Microbiol 8:922

Falkowski PG, Raven JA (2007) Aquatic photosynthesis. Princeton University Press, New Jersey

Fulda S, Gorman AM, Hori O, Samali A (2010) Cellular stress responses: cell survival and cell death. Int J Cell Biol 2010:214074

Gross M, Zhao X, Mascarenhas V, Wen Z (2016) Effects of the surface physico-chemical properties and the surface textures on the initial colonization and the attached growth in algal biofilm. Biotechnol Biofuels 9:38

Guillard RRL (1975) Culture of phytoplankton for feeding marine invertebrates. In: Smith WL, Chanley MH (eds) Culture of marine invertebrate animals: Proceedings—1st conference on culture of marine invertebrate animals greenport. Springer, Boston, pp 29–60

Guinder VA, Molinero JC (2013) Climate change effects on marine phytoplankton. In: Arias AH, Menéndez MC (eds) Marine ecology in a changing world. CRC Press-Taylor & Francis, Boca Raton, pp 68–90

Guo R, Youn SH, Ki J-S (2015) Heat Shock Protein 70 and 90 genes in the harmful dinoflagellate *Cochlodinium polykrikoides*: genomic structures and transcriptional responses to environmental stresses. Int J Genomics 2015:e484626

Häder D-P, Gao K (2015) Interactions of anthropogenic stress factors on marine phytoplankton. Front Environ Sci 3:14

Hays GC, Richardson AJ, Robinson C (2005) Climate change and marine plankton. Trends Ecol Evol 20:337–344

Huertas IE, Rouco M, López-Rodas V, Costas E (2011) Warming will affect phytoplankton differently: evidence through a mechanistic approach. Proc Roy Soc B 278:3534–3543

Hunter KA, Liss PS (1981) Polarographic measurement of surface-active material in natural waters. Water Res 15:203–215

Israelachvili JN (1992) Intermolecular forces & surface forces. Academic Press, New York

Ivošević N, Tomaić J, Žutić V (1994) Organic droplets at an electrified interface: critical potentials of wetting measured by polarography. Langmuir 7:2415–2418

Ivošević N, Žutić V (1997) Polarography of marine particles: a model study. Croat Chem Acta 70:167–178

Ivošević DeNardis N, Žutić V, Svetličić V, Frkanec R, Tomašić J (2007) In situ amperometric characterization of liposome suspensions with concomitant oxygen reduction. Electroanalysis 19:2444–2450

Ivošević DeNardis N, Pečar Ilić J, Ružić I, Novosel N, Mišić Radić T, Weber A, Kasum D, Pavlinska P, Katalin Balogh R, Hajdu B, Marček Chorvátová A, Gyurcsik B (2019) Algal cell response to laboratory-induced cadmium stress: a multimethod approach. Eur Biophys J 48:231–248

Katz A, Waridel P, Shevchenko A, Pick U (2007) Salt-induced changes in the plasma membrane proteome of the halotolerant alga *Dunaliella salina* as revealed by blue native gel electrophoresis and nano-LC-MS/MS analysis. Mol Cell Proteomics 6:1459

Kim S-K (ed)(2015) Handbook of marine microalgae. Academic Press, London

Klenerman D, Korchev YE, Davis SJ (2011) Imaging and characterisation of the surface of live cells. Curr Opin Chem Biol 15:696–703

Kobiyama A, Tanaka S, Kaneko Y, Lim P-M, Ogata T (2010) Temperature tolerance and expression of heat shock protein 70 in the toxic dinoflagellate *Alexandrium tamarense* (Dinophyceae). Harmful Algae 9:180–185

Kovač S, Svetličić V, Žutić V (1999) Molecular adsorption vs. cell adhesion at an electrified aqueous interface. Colloids Surf A 149:481–489

Kovač S, Kraus R, Geček S, Žutić V (2000) Cell suspension as a model system for electrochemical analysis. Croat Chem Acta 73:279–291

Kumar D, Kvíderová J, Kaštánek P, Lukavský J (2017) The green alga *Dictyosphaerium chlorelloides* biomass and polysaccharides production determined using cultivation in crossed gradients of temperature and light. Eng Life Sci 17:1030–1038

Lane TW, Saito MA, George GN, Pickering IJ, Prince RC, Morel FM (2005) A cadmium enzyme from a marine diatom. Nature 435:42

Lewandowska A, Sommer U (2010) Climate change and the spring bloom: a mesocosm study on the influence of light and temperature on phytoplankton and mesozooplankton. Mar Ecol Prog Ser 405:101–111

Los DA, Mironov KS, Allakhverdiev SI (2013) Regulatory role of membrane fluidity in gene expression and physiological functions. Photosynth Res 116:489–509

Lyon BR, Mock T (2014) Polar microalgae: New approaches towards understanding adaptations to an extreme and changing environment. Biology 3:56–80

Martignier A, Filella M, Pollok K, Melkonian M, Bensimon M, Barja F, Langenhorst F, Jaquet J-M, Ariztegui D (2018) Marine and freshwater micropearls: biomineralization producing strontium-rich amorphous calcium carbonate inclusions is widespread in the genus *Tetraselmis* (Chlorophyta). Biogeosciences 15:6591–6605

Mata JA, Béjar V, Llamas I, Arias S, Bressollier P, Tallon R, Urdaci MC, Quesada E (2006) Exopolysaccharides produced by the recently described halophilic bacteria *Halomonas ventosae* and *Halomonas anticariensis*. Res Microbiol 157:827–835

Mayali X, Franks PJS, Tanaka Y, Azam F (2008) Bacteria-induced motility reduction in *Lingulodinium polyedrum* (Dinophyceae). J Phycol 44:923–928

Mishra A, Kavita K, Jha B (2011) Characterization of extracellular polymeric substances produced by micro-algae *Dunaliella salina*. Carbohydr Polym 83:852–857

Mišić Radić T, Čačković A, Penezić A, Dautović J, Lončar J, Omanović D, Juraić K, Ljubešić Z (2020) Physiological and morphological response of marine diatom *Cylindrotheca closterium* (Bacillariophyceae) exposed to cadmium. Eur J Phycol 24:36

Novosel N, Kasum D, Žutinić P, Legović T, Ivošević DeNardis N (2020) Short-term effect of cadmium on the motility of three flagellated algal species. J Appl Phycol 32:4057–4067

Novosel N, Ivošević DeNardis N (2021) Structural features of the algal cell determine adhesion behavior at a charged interface. Electroanalysis 33:1436–1443

Ozkan A, Berberoglu H (2013) Physico-chemical surface properties of microalgae. Colloids Surf B 112:287–293

Pavlinska Z, Chorvat D, Mateasik A, Jerigova M, Velic D, Ivošević DeNardis N, Marcek Chorvatova A (2020) Fluorescence responsiveness of unicellular marine algae *Dunaliella* to stressors under laboratory conditions. J Biotechnol 6:100018–100028

Pillet F, Dague E, Pečar Ilić J, Ružić I, Rols M-P, Ivošević DeNardis N (2019) Changes in nanomechanical properties and adhesion dynamics of algal cells during their growth. Bioelectrochemistry 128:154–162.

Pletikapić G, Berquand A, Mišić Radić T, Svetličić V (2012) Quantitative nanomechanical mapping of marine diatom in seawater using peak force tapping atomic force microscopy. J Phycol 48:174–185

Pletikapić G, Ivošević DeNardis N (2017) Application of surface analytical methods for hazardous situation in the Adriatic sea: monitoring of organic matter dynamics and oil pollution. Nat Hazards Earth Syst Sci 17:31–44

Ras M, Steyer J-P, Bernard O (2013) Temperature effect on microalgae: a crucial factor for outdoor production. Rev Environ Sci Biotechnol 12:153–164

Riebesell U (1991) Particle aggregation during a diatom bloom II. Biological Aspects Mar Ecol Prog Ser 69:281–291

Ritossa F (1996) Discovery of the heat shock response. Cell Stress Chaperon 2:97–98

Roncarati F, Rijstenbil JW, Pistocchi R (2008) Photosynthetic performance, oxidative damage and antioxidants in *Cylindrotheca closterium* in response to high irradiance, UVB radiation and salinity. Mar Biol 153:965–973

Sader JE, Larson I, Mulvaney P, White LR (1995) Method for the calibration of atomic force microscope cantilevers. Rev Sci Instrum 66:3789–3798

Sarmiento JL, Slater R, Barber R, Bopp L, Doney SC, Hirst AC, Kleypas J, Matear R, Mikolajewicz U, Monfray P, Soldatov V, Spall SA, Stouffer R (2004) Response of ocean ecosystems to climate warming. Global Biogeochem Cycl 18:1–23

Sneddon IN (1965) The relation between load and penetration in the axisymmetric boussinesq problem for a punch of arbitrary profile. Int J Eng Sci 3:47–57

Svetličić V, Ivošević N, Kovač S, Žutić V (2000) Charge displacement by adhesion and spreading of a cell: amperometric signals of living cells. Langmuir 16:8217–8220

Svetličić V, Ivošević N, Kovač S, Žutić V (2001) Charge displacement by adhesion and spreading of a cell. Bioelectrochemistry 53:79–86

Svetličić V, Balnois E, Žutić V, Chevalet J, Hozić Zimmermann A, Kovač S, Vdović N (2006) Electrochemical detection of gel microparticles in seawater. Croat Chem Acta 79:107–113

Thornton D (2002) Diatom aggregation in the sea: mechanisms and ecological implications. Eur J Phycol 37:149–161

Urbani R, Magaletti E, Sist P, Cicero AM (2005) Extracellular carbohydrates released by the marine diatoms *Cylindrotheca closterium*, *Thalassiosira pseudonana* and *Skeletonema costatum*: Effect of P-depletion and growth status. Sci Total Environ 353:300–306

Wolfstein K, de Brouwer JFC, Stal LJ (2002) Biochemical partitioning of photosynthetically fixed carbon by benthic diatoms during short-term incubations at different irradiances. Mar Ecol Prog Ser 245:21–31

Xia L, Huang R, Li Y, Song S (2017) The effect of growth phase on the surface properties of three oleaginous microalgae (*Botryococcus* sp. FACGB-762, *Chlorella* sp. XJ-445 and *Desmodesmus bijugatus* XJ-231). PloS One 12:e0186434

Žutić V, Kovač S, Svetličić V (1993) Heterocoalescence between organic microdroplets and charged conductive interface. J Electroanal Chem 349:173–186

Žutić V, Svetličić V, Ivošević N, Hozić A, Pečar O (2004) Northern Adriatic mesocosm experiment Rovinj 2003: dynamics of organic microparticles studied by the electrochemical technique. Period Biol 106:67–74